Official Journal of the World Water Council
Water Policy

Water Policy Vol 23 No 4, 1059 doi: 10.2166/wp.2021.193

Study on the influence of infiltration on flood propagation with different peak shape coefficients and duration

Jingming Hou[a], Zhaoan Zhang[a,*], Dawei Zhang[b], Baoshan Shi[a], Guangzhao Chen[a] and Hongbin Zhang[b]

[a] State Key Laboratory Eco-hydraulics Northwest Arid Region of China, Xi'an University of Technology, Xian, 710048 Shaanxi, China
[b] China Institute of Water Resources and Hydropower Research, Beijing 100038, China
*Corresponding author. E-mail: zzazax@hotmail.com

ABSTRACT

Traditional flood simulations fail to properly consider the impact of soil infiltration in floodplain areas with high soil infiltration rates. Notably, ignoring soil infiltration will lead to considerable uncertainty in flood simulations. In this paper, a fully hydrodynamic model coupled with the Green–Ampt infiltration model was used. Taking a natural reach in northern China (HTH in this paper) as a case study, observed flood discharge data were used to analyze the influence of soil infiltration on flood propagation based on the flood propagation simulation results for various inflow conditions. The maximum difference of inundation area is about 25%. The results show that soil infiltration has little effect on the inundation area during the rising stage of a flood. In the late period of a flood, the inundation area considering the effect of infiltration is smaller than that without infiltration, and the smaller the peak coefficient is, the longer the flood duration is, the larger the impact of infiltration on the inundation area. When the peak shape coefficient is 0.42 and the flood duration is 44.4 h, the maximum difference of the inundation area is about 28%. The research results provide a reference for flood management and post-disaster rescue efforts.

Key words: Flood propagation, Green–Ampt model, Hydrodynamic model, Infiltration, Inundation area, Peak shape coefficient

HIGHLIGHTS

- Using a fully hydrodynamic model coupled with the Green–Ampt model to simulate the flood propagation.
- The model uses graphic processing unit acceleration technology.
- Analyzing the influence of soil infiltration on flood based on the flood propagation simulation results.
- It is considered that the flood peak shape coefficient has influence on infiltration.
- The results provide a reference for flood management and post-disaster rescue efforts.

GRAPHICAL ABSTRACT

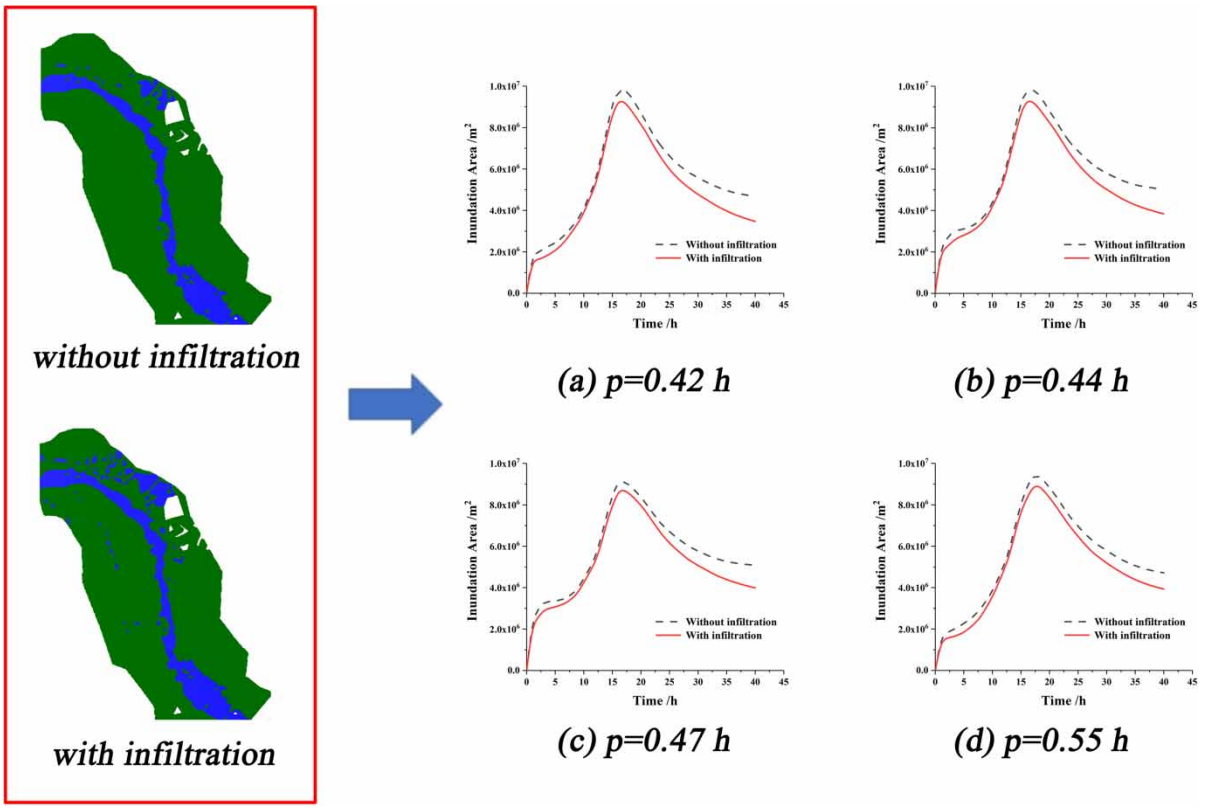

1. INTRODUCTION

One of the most well-known definitions of vulnerability to climate change was presented in the Intergovernmental Panel on Climate Change (IPCC) Third Assessment Report (Climate Change 2001: Mitigation, 2002) as the degree to which a system is exposed, sensitive to and/or unable to cope with adverse effects of climate change. In recent years, with the frequent occurrence of extraordinary weather worldwide, such as heavy rainstorms and hail, secondary disasters caused by unusual weather, such as debris flows and mountain torrents, are also increasing in frequency (Westra *et al.*, 2014; Wu *et al.*, 2014; Valipour *et al.*, 2020). These disaster events can be harmful to human life, and economic losses can be extensive (Marchi *et al.*, 2010; Hou *et al.*, 2020b). Notably, fluvial floods are among the major natural disasters that occur, and inundated areas are important for fluvial flood impact assessments (Dutta *et al.*, 2006; Hou *et al.*, 2019). Many factors affect an inundated area, such as the flood duration, flood peak and flood volume. However, infiltration is also an important factor, and it is often ignored in the numerical simulation of floods. When floods occur, infiltration is one of the main factors that result in water volume loss in some areas with large infiltration values. To accurately predict the flood risk, we should consider the effects of infiltration.

Hydrodynamic models, such as those proposed by Bazilevs *et al.* (2011), Liang (2010), Jeong *et al.* (2012), Hou *et al.* (2013a), Ata *et al.* (2013) and Guan *et al.* (2014), play a significant role in quantitatively evaluating flood risk. Although these models can simulate flood propagation, soil infiltration is not taken into account.

The most common infiltration methods in hydrology are Philip, Horton and Green–Ampt (G-A) methods (Fernández-Pato *et al.*, 2016). Among them, the advantage of the G-A model is that its parameters have definite physical meaning, which helps establish the relationships between characteristic parameters and physical soil characteristics (Meng & Yang, 2019). This model is also accurate, so most scholars have accepted it. Notably, the G-A model is applied to study homogeneous soil, layered soil, muddy water and intermittent infiltration and to determine the relationship between the infiltration rate and soil characteristics. The formula is simple, and the calculations are convenient. Especially for long-term infiltration, the calculation accuracy is relatively high. Chu (1978) extended the improved G-A model to an analysis of rainfall infiltration processes with naturally variable rainfall intensities, which made the G-A model applicable to calculations of infiltration for heterogeneous rainfall patterns, thus broadening the application scope of the G-A model; this improved approach has been commonly used to simulate rainfall infiltration and runoff processes in sloped areas (Esteves *et al.*, 2000; Simons *et al.*, 2014). Fernández-Pato *et al.* (2016) used a model based on two-dimensional shallow water equations (SWEs) to simulate the rainfall–runoff relationship and to analyze and correct the sensitivity of infiltration parameters.

Most of the above studies only consider the hydrodynamic process, and it does not consider the impact of hydrological processes, such as evaporation and infiltration on flood routing (Liang 2010; Bazilevs *et al.*, 2011; Jeong *et al.*, 2012; Ata *et al.*, 2013; Hou *et al.*, 2013a; Guan *et al.*, 2014). Or only the G-A model is studied to determine its participation and scope of application (Esteves *et al.*, 2000; Simons *et al.*, 2014; Fernández-Pato *et al.*, 2016; Meng & Yang, 2019). Besides, the influence of infiltration on a flood plain, including the inundation duration and the inundation area (Fernández-Pato *et al.*, 2016), is not considered, and the model used for the study is relatively simple and the computational efficiency is not high. In this work, to study the flood submergence behaviors of floodplains considering the impact of infiltration, a dynamic wave-based high-performance distributed hydrological model was used to simulate flood propagation routing under different inflow conditions. This hydrologic model is coupled with the hydrodynamic model. The method of rainfall intensity minus infiltration rate, evapotranspiration rate and interception rate was used to describe the runoff generation process. Infiltration, evapotranspiration and interception were considered in every cell by the Hargreaves method, the A.P.J.D E ROO method and the G-A model, respectively. To enable large-scale high-resolution simulations, the computation is accelerated with high-performance graphic processing units (GPUs) and a parallel computing technique. The model can accurately simulate the flood propagation process, and with high-resolution topography input data, the simulation efficiency can be guaranteed. In this study, only the surface water module and the G-A infiltration module of the model have been applied. This paper is structured as follows: the research methods and models are introduced in Section 2; subsequently, the effects of infiltration on floodplains are analyzed under different inflow conditions in Sections 3–5; and finally, brief conclusions are drawn in Section 6.

2. METHODOLOGY

To study the flood submergence law of floodplains considering infiltration, a numerical model based on a two-dimensional dynamic wave method coupled with hydrological and hydrodynamic processes was developed. The G-A model was used to calculate infiltration loss, and the fully hydrodynamic numerical model was used to simulate the flood propagation process.

2.1. High-resolution hydrodynamic model

The GAST (GPU Accelerated Surface Water Flow and Associated Transport) model is a fully hydrodynamic model based on GPU acceleration techniques. A high-resolution digital elevation model (DEM) is applied as the basic data source to solve the SWEs in the framework of a Godunov-type finite volume scheme. To accurately

predict the flood inundation process, the realistic features of the terrain are resolved, and a GPU parallel computing technology was used to accelerate calculation (Hou *et al.*, 2020a).

2.1.1. Governing equations

The governing equations of the GAST model are the SWEs, which are derived from the depth integration of the Navier–Stokes equations assuming a hydrostatic pressure distribution. In this model, the kinetic and turbulent viscous terms, wind stresses and Coriolis effects are neglected, and the conservation law of the two-dimensional nonlinear SWEs can be written in vector form as follows (Hou *et al.*, 2020c):

$$\frac{\partial q}{\partial t}+\frac{\partial f}{\partial x}+\frac{\partial g}{\partial y}=S \tag{1}$$

$$q=\begin{bmatrix} h \\ q_x \\ q_y \end{bmatrix},\ f=\begin{bmatrix} uh \\ uq_x+gh^2/2 \\ uq_y \end{bmatrix},\ g=\begin{bmatrix} vh \\ vq_x \\ vq_y+gh^2/2 \end{bmatrix} \tag{2}$$

$$S=\begin{bmatrix} i \\ -\dfrac{gh\partial z_{\mathrm{b}}}{\partial x}-C_{\mathrm{f}}u\sqrt{u^2+v^2} \\ -\dfrac{gh\partial z_{\mathrm{b}}}{\partial y}-C_{\mathrm{f}}v\sqrt{u^2+v^2} \end{bmatrix} \tag{3}$$

where t represents the time; x and y are the Cartesian coordinates; q denotes the vector of conserved flow variables consisting of h, q_x, and q_y, which are the water depth and unit-width discharges in the x- and y-directions, respectively; $q_x = uh$ and $q_y = vh$, where u and v are the depth-averaged velocities in the x- and y-directions; f and g represent the flux vectors in the x- and y-directions, respectively; S is the source vector, which can be further subdivided into a slope source term Sb and a friction source term S_{f}; z_{b} represents the bed elevation; C_{f} is the bed roughness coefficient, which is generally computed by $gn^2/h^{1/3}$, with n being the Manning coefficient; i is the mass source or sink term and is equal to $i_{\mathrm{r}} - i_{\mathrm{i}}$, where i_{r} is the rainfall rate and i_{i} denotes the infiltration rate. When the rainfall rate i_{r} is larger than the infiltration rate i_{i}, i is a source term, and vice versa in this case when i is a sink term. Moreover, the water level $\eta = h + z_{\mathrm{b}}$ is also used in the numerical scheme adopted in this work.

This section describes the numerical model for solving the SWEs within the framework of a Godunov-type cell-centered finite volume scheme based on structured grids. The SWEs are discretized into algebraic equations by the finite volume method. The fluxes of mass and momentum are computed by the HLLC (Harten Lax van Leer Contact) approximate Riemann solver (i.e., Harten, Lax and van Leer approximate Riemann solver with the contact wave restored). The slope source terms are evaluated by the slope flux method proposed by Hou *et al.* (2013b). The friction source terms are calculated with an improved explicit method. When computing the fluxes and the slope source terms, the values at the midpoints of the cell edges are required. The two-stage explicit Runge–Kutta approach is applied to update the flow variables to a new time level (Hou *et al.*, 2018). These values are evaluated with a novel 2D edge-based MUSCL (Monotonic Upwind Scheme for Conservation Laws) scheme.

2.1.2. Infiltration

The G-A conception of the infiltration process is one in which infiltrated water moves vertically downward in a saturated layer, beginning at the surface (Hou *et al.*, 2018). To describe the characteristics of soil water

infiltration, the G-A infiltration model was applied according to the basic assumptions (Hsu & Hilpert, 2011).

$$f_p = \begin{cases} R & t \le t_p \\ K_s[1 + (\theta_s - \theta_i)S_f/I_p] & t > t_p \end{cases} \quad (4)$$

where f_p represents the infiltration rate; K_s is the saturated hydraulic conductivity; θ_i and θ_s are initial soil moisture and saturated water content, respectively; S_f represents humid front suction; t_p represents the start time of inundation after rainfall begins; R is the rainfall intensity; and I_p is cumulative infiltration, where $I_p = t_p R$.

2.2. Model validation

2.2.1. Validation area and model set

The validation area is Morpeth in Northeast England, UK. The Wansbeck River in the urban region of Morpeth is a flood-prone area with many floods historically. Between the 4th and 6th of September 2008, rainfall with a 137-year return period occurred in Northeast England. The catchment was already almost saturated from the antecedent rainfall in July and August, which caused surface runoff and rising river levels and flows (Lamb *et al.*, 2009).

The input data for the model were divided into inflow data, topographic data and hydrology-related parameters. The discharge process is shown in Figure 1. The terrain of this model is based on the 5-m DEM data provided by the local environmental protection department. The DEM has 52,200 (290×180) grids in total (Figure 2). According to local conditions, Manning's roughness coefficient is set to 0.02 $m^{1/3}$·s, and the Courant number is 0.5. The upstream boundary of the model is an inflow boundary, and the downstream boundary is an open boundary; the rest of the model has a closed boundary. A result file is output every 1 h.

According to the Soil Site Report of the National Soil Resources Institute, the soil types in Morpeth are clay loam and sandy clay loam. Because the sandy clay loam only accounts for 4% of the soil in mopes, the proportion is very small of the soil in Morpeth, it is not considered in this simulation. General G-A infiltration parameters can be obtained from the USDA (United States Department of Agriculture) soil texture classification (Rawls *et al.*, 1982).

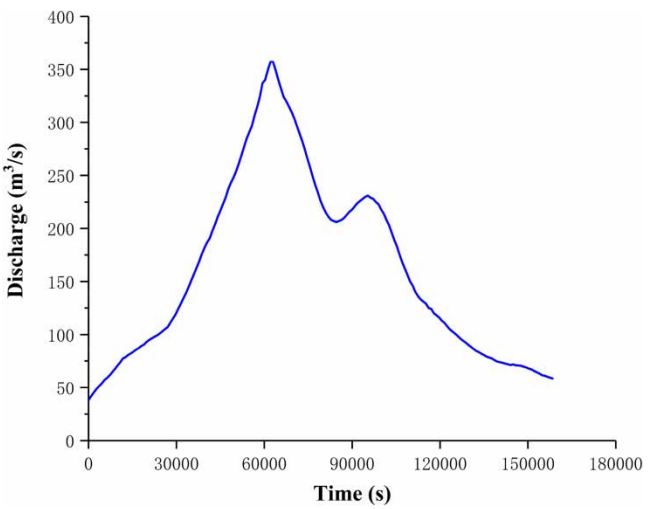

Fig. 1. | The discharge data for Morpeth from 4 to 11 September 2008.

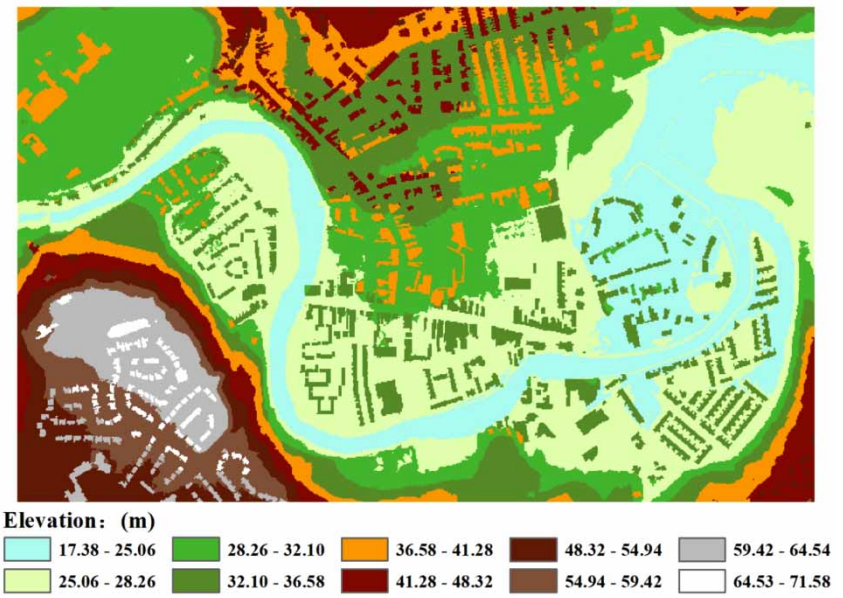

Fig. 2. | 5 m × 5 m DEM of Morpeth in England.

Because the soil was almost saturated prior to the flood event, the initial moisture content was set equal to the saturated moisture content in the model. Thus, the only parameter that affects infiltration is the saturated hydraulic conductivity (K_s). In this case, K_s is 0.1 cm/h (Zhang, 2014).

2.2.2. Validation result

After the flood in 2008, the local environmental protection department organized a flood survey to collect water depth data at over 2,000 points, and the measured inundation map of the urban area reflecting the maximum inundation range of the flood was obtained through inverse distance interpolation (Figure 3).

According to Figure 3, there are four main flooded areas: A, B, C and D. The simulated inundation area of these four areas is compared with the measured inundation area in Table 1. The results show that the relative error between the measured value and the simulated value in each block is no greater than 0.8%. Additionally, the average relative error is 0.75%, which suggests that the model can effectively simulate the flood process in floodplain areas.

3. STUDY AREA AND DATA

3.1. Study area

The study area is a natural reach in northern China (HTH in this paper), which is located in a warm temperate zone within a semi-humid continental monsoon climate region. The rainy season is concentrated from July to August. During the rainy season, the river is full, the river banks are generally flooded and serious flood disasters occur. In addition to the bare land in tidal flat areas, there is cultivated land in some nearby villages and some industrial and mining enterprises. When floods occur, they often threaten the lives, property and security of local residents.

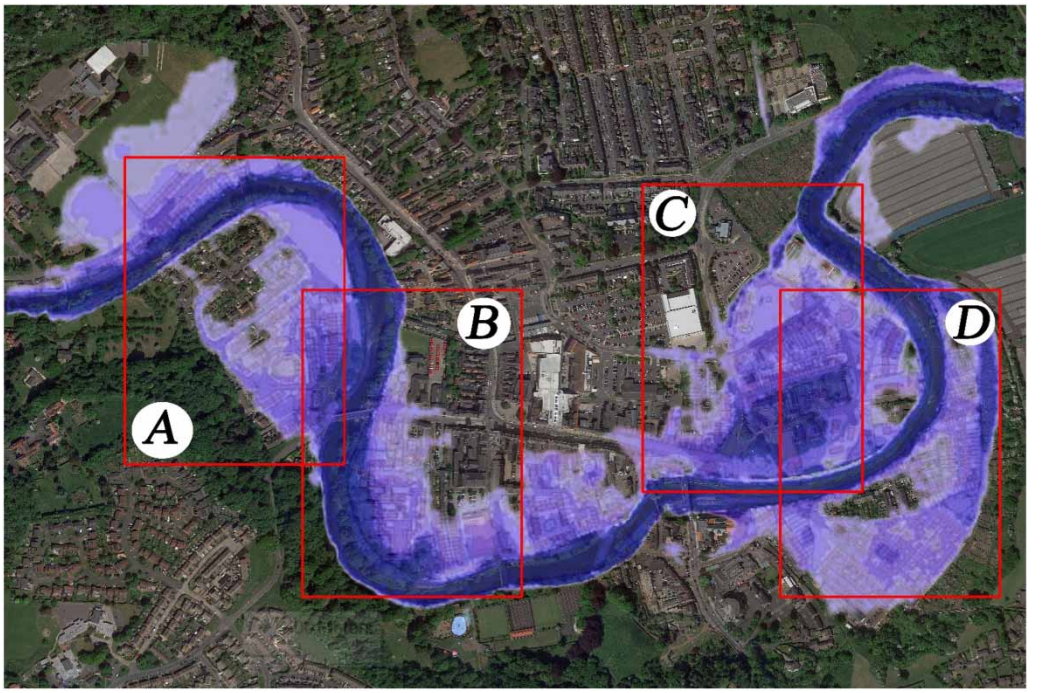

Fig. 3. | Maximum inundation range measured in urban areas.

Table 1. | The results of validation.

Area	Measurement results (m^2)	Simulation results (m^2)	Relative error (%)
A	78,156	78,668	0.66
B	57,397	57,858	0.8
C	76,206	76,811	0.79
D	112,404	113,229	0.73

3.2. Data and parameter setting

The model input data are divided into inflow data, topographic data and data for hydrology-related parameters. The inflow data will be discussed in a specific example. The study area is about 52 km^2, the length of the river is about 13 km and the average longitudinal slope is about 2.5‰. The river bed is 500–1,000 m wide, and the river channel is gentle. There are water storage project, water diversion project, water lifting project, water diversion project and water wells in the upstream and downstream of the study area, so as to control and utilize the flood. The terrain of this model is based on the DEM data provided by the China Institute of Water Resources and Hydropower Research (Figure 4). The DEM has 1,132,544 ($896 \times 1{,}264$) grids in total, and the grid size is 10 m $\times$ 10 m.

According to local conditions, the Manning coefficients of different land uses are based on those of Engman & Asce (1986), and infiltration is based on the G-A model with parameters, which are from Li & Zheng (2008). To facilitate the calculations, the buildings in the terrain are removed, the river channel is regarded as having no

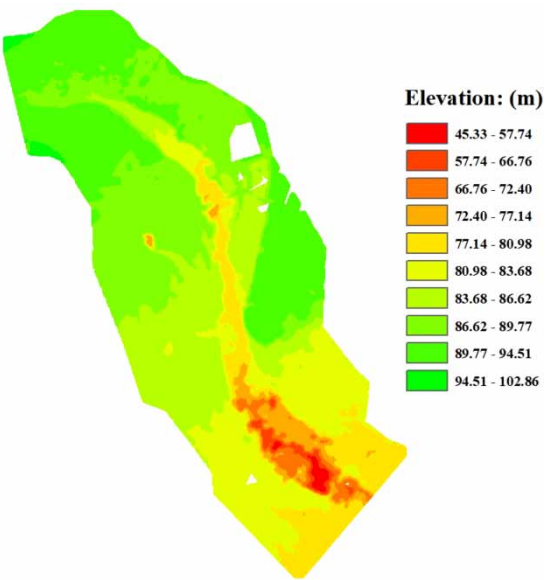

Fig. 4. | 10 m × 10 m DEM of HTH.

infiltration and other areas are treated as bare land. The Manning's roughness coefficient is set to 0.02 $m^{1/3}$·s, and the saturated hydraulic conductivity and capillary force of bare land are 0.005 cm/s and 4.21 cm, respectively (Yanwei *et al.*, 2015).

The Courant number is 0.5. The upstream boundary of the model is an inflow boundary, the downstream boundary is an open boundary and all other boundaries are closed boundaries. All test cases were run with a GPU (NVIDIA GeForce GTX 1080) to improve the computing efficiency. All of the designed floods are based on the actual flood discharge in this paper.

4. RESULTS

There are many criteria for evaluating the impact of flood propagation, such as the flooded area, flooded depth and flood duration. This study estimates flood propagation through simulations under various inflow conditions and determines the relation between infiltration and the flooded area to explore whether it is necessary to consider infiltration factors when the model is used to simulate the flood risk. In this hydrodynamic model, the influence of infiltration is reflected in the i of Equation (3), which affects the water depth in the grid. The peak shape coefficient and flood duration mentioned later play an important role in the left three terms of Equation (1), which affect the water depth and velocity in the calculation grid.

In this paper, the peak shape coefficient and flood duration are used to control different designed floods. The peak shape coefficient reflects the shape before the flood peak. When the flood peak, flood volume and flood duration are fixed, the flood control situation is determined based on the flood pattern. Therefore, it is necessary to consider the shape (peak shape coefficient) in flood simulation.

$$p = \frac{1/t_p \int_0^{t_p} Q_t dt}{Q_p} \tag{5}$$

where p represents the peak shape coefficient; t_p is the corresponding time when the flood peak appears; Q_t is the flood discharge at time t; and Q_p is the flood peak discharge.

4.1. Effects of different peak shape coefficients on flood propagation considering the infiltration process

This case simulated the effect of infiltration on the inundation area under the conditions that the flood duration remained unchanged and the peak shape coefficient changed. Figure 5 shows the different inflow conditions. The four situations are $p = 0.42$, $p = 0.44$, $p = 0.47$ and $p = 0.55$, and all flood durations are 144,000 s. The simulation time is 144,000 s, the output interval is 3,600 s and the values of other parameters were described in Section 3.2.

Figure 6 shows the simulation results for differently designed flood discharge hydrographs, which indicate that the inundation area changes with time throughout the flooding process. We can conclude that infiltration has little effect on the flood inundation area of the floodplain in the rising stage of a flood. However, in the recession stage, the influence of infiltration is notable, and as the recession stage continues, the influence of infiltration gradually increases. Significant differences can be seen in the red box area in Figure 7 (because the lower reaches of the river are deep, no obvious floodplain occurs and the difference is small). This result is reflected by the four peak shape coefficients.

In this study, the change in the inundation area caused by floods is compared when flood propagation is simulated with and without infiltration. The inundated area at the end of the flood is selected for comparison, and the results are shown in Table 2.

$$\Delta = \frac{|S_{ni} - S_i|}{S_{ni}} \times 100\% \tag{6}$$

where Δ is the relative error, S_{ni} is the inundation area without infiltration, and S_i is the inundation area with infiltration.

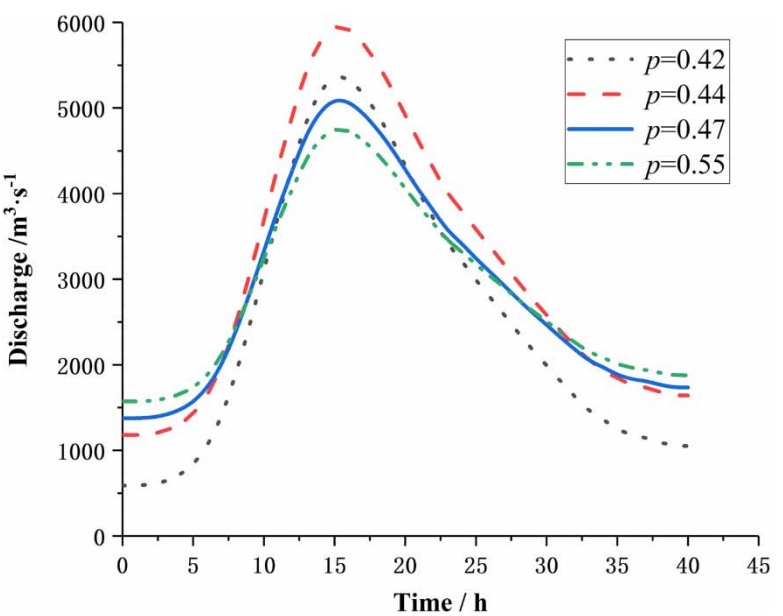

Fig. 5. | Designed flood hydrograph.

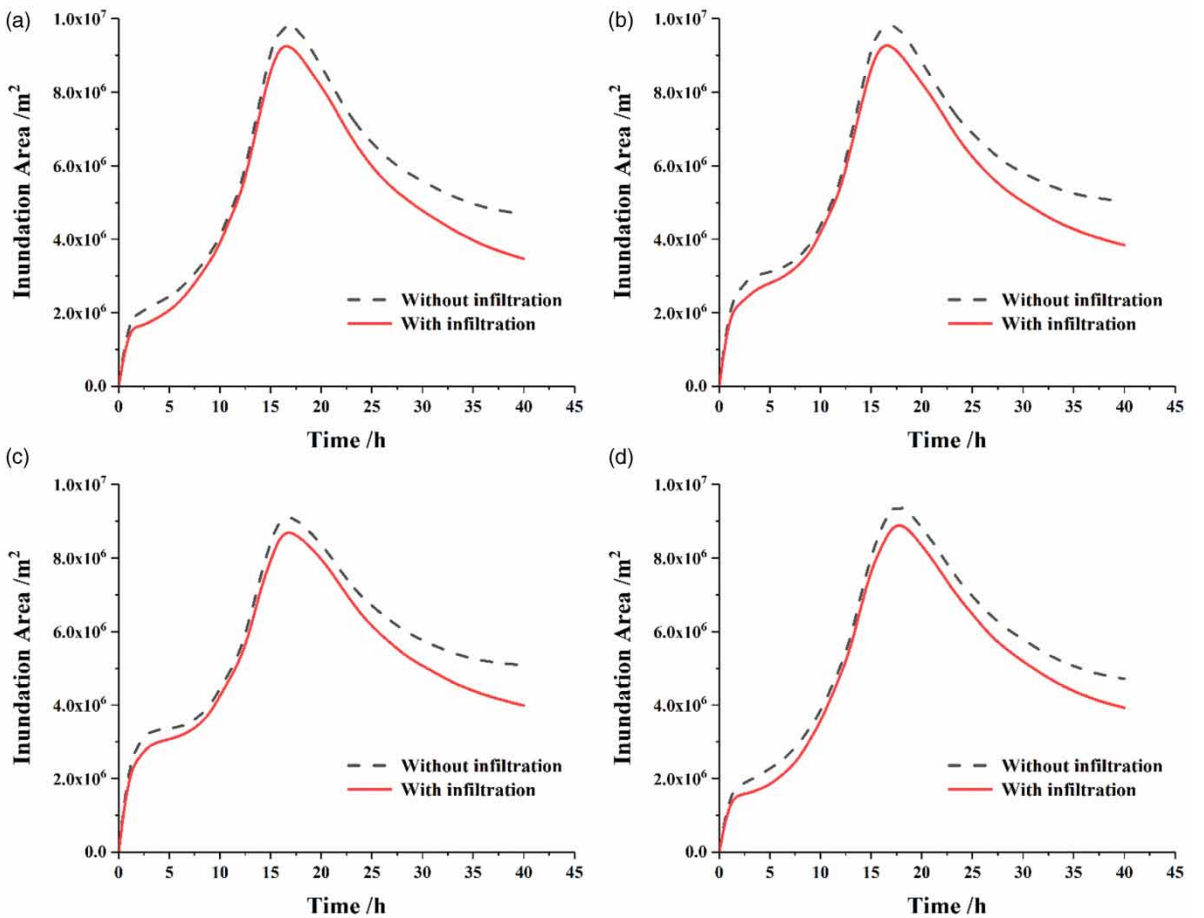

Fig. 6. | Inundation area computed by the model with/without the infiltration process: (a) $p = 0.42$; (b) $p = 0.44$; (c) $p = 0.47$; and (d) $p = 0.55$.

From Table 2, when the peak shape coefficient is 0.42, the relative error is 24.59%. As the peak shape coefficient increases, the flood type becomes a 'short and fast flood' type, and the difference in the inundated area between the two cases decreases. When the peak shape coefficient is increased to 0.55, the relative error decreases to 20.30%.

4.2. Effects of different flood durations on flood propagation considering the infiltration process

The G-A model is a hydrological model, and the simulated infiltration process is slow. Therefore, the flood duration may be an important variable that influences the infiltration effect.

This case simulated the influence of infiltration on the inundation area under situations in which the peak shape coefficient remained unchanged and the flood duration changed. Figure 8 shows the different inflow situations. The four flood durations are $t = 40{,}000$, $t = 80{,}000$, $t = 120{,}000$ and $t = 160{,}000$ s, and all the peak shape coefficients are 0.42 h. The other parameter settings are described in Section 3.2.

Figure 9 shows the simulation results for differently designed flood discharge hydrographs. Notably, the inundation area changes throughout the flood propagation process. Figure 9 shows a similar pattern as that in

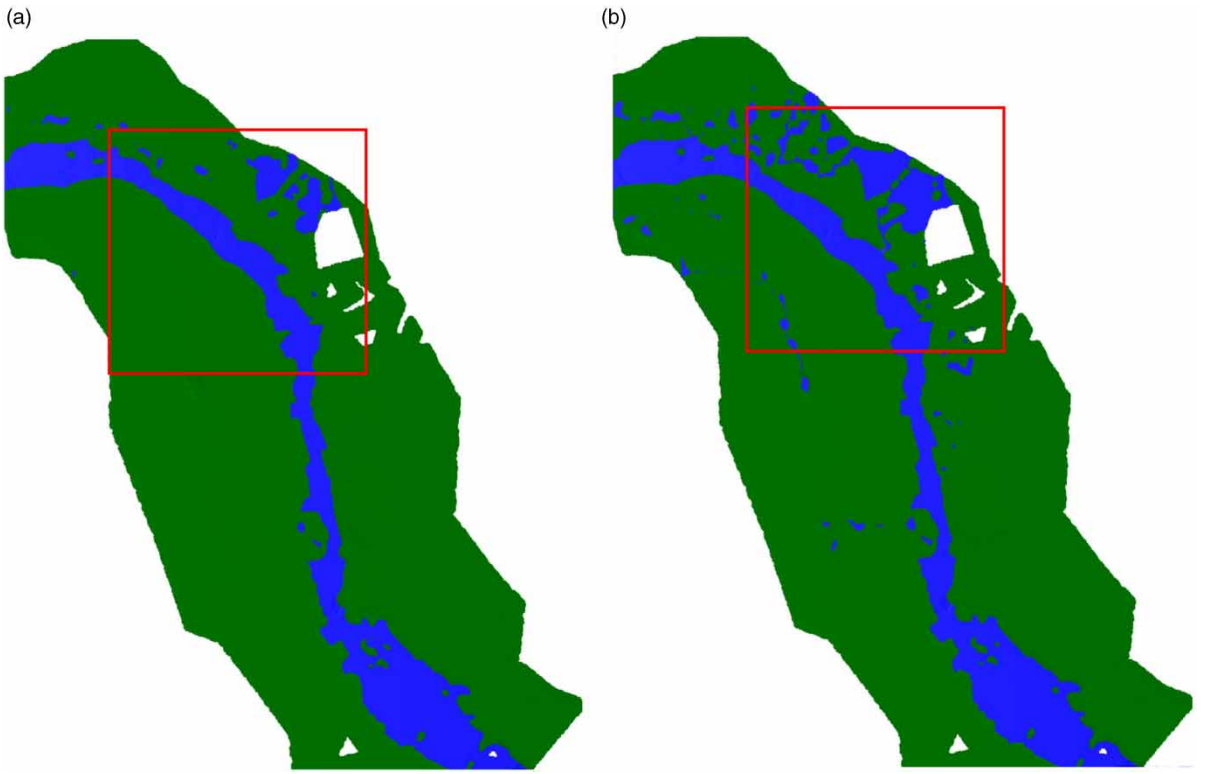

Fig. 7. | Simulation results for the flood inundation area at 72,000s ($p = 0.42$): (a) without infiltration and (b) with infiltration. Please refer to the online version of this paper to see this figure in colour: http://dx.doi.org/10.2166/wp.2021.193.

Table 2. | Comparison of the inundation areas computed by the models with/without the infiltration process.

Peak shape coefficient (h)	0.42	0.44	0.47	0.55
Relative error (%)	25.98	23.59	21.48	20.40

Figure 6. The infiltration trend is different from the inundation area pattern in the flood recession stage. As a flood progresses, the influence of infiltration gradually increases. This trend is also observed for each flood duration.

Using the same analysis method as in Section 4.1, Table 3 shows that for the four flood durations, when the flood durations is 1.11 h, the relative error is 12.54%. As the flood duration increases, the difference in the inundated area between the two cases increases. When the flood duration is increased to 44.4 h, the relative error decreases to 28.20%.

5. DISCUSSION

The simulation results in Section 4 show that the inundation area changes with the flooding process. When the flood rises, the flow in the river increases gradually, and the water overflows both banks, making the beach and

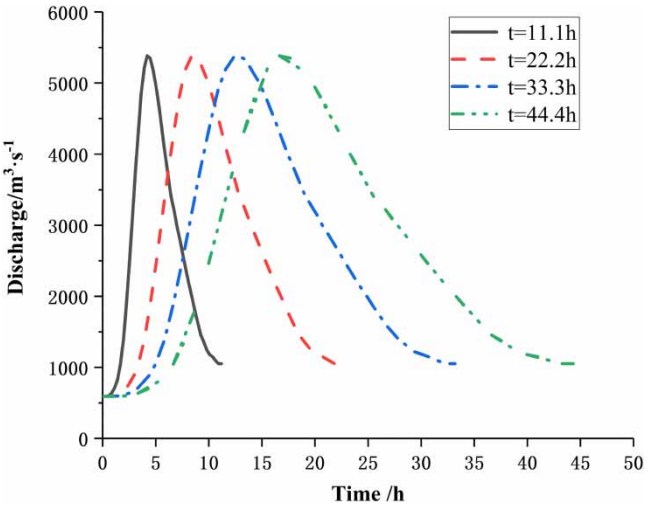

Fig. 8. | Designed flood hydrograph.

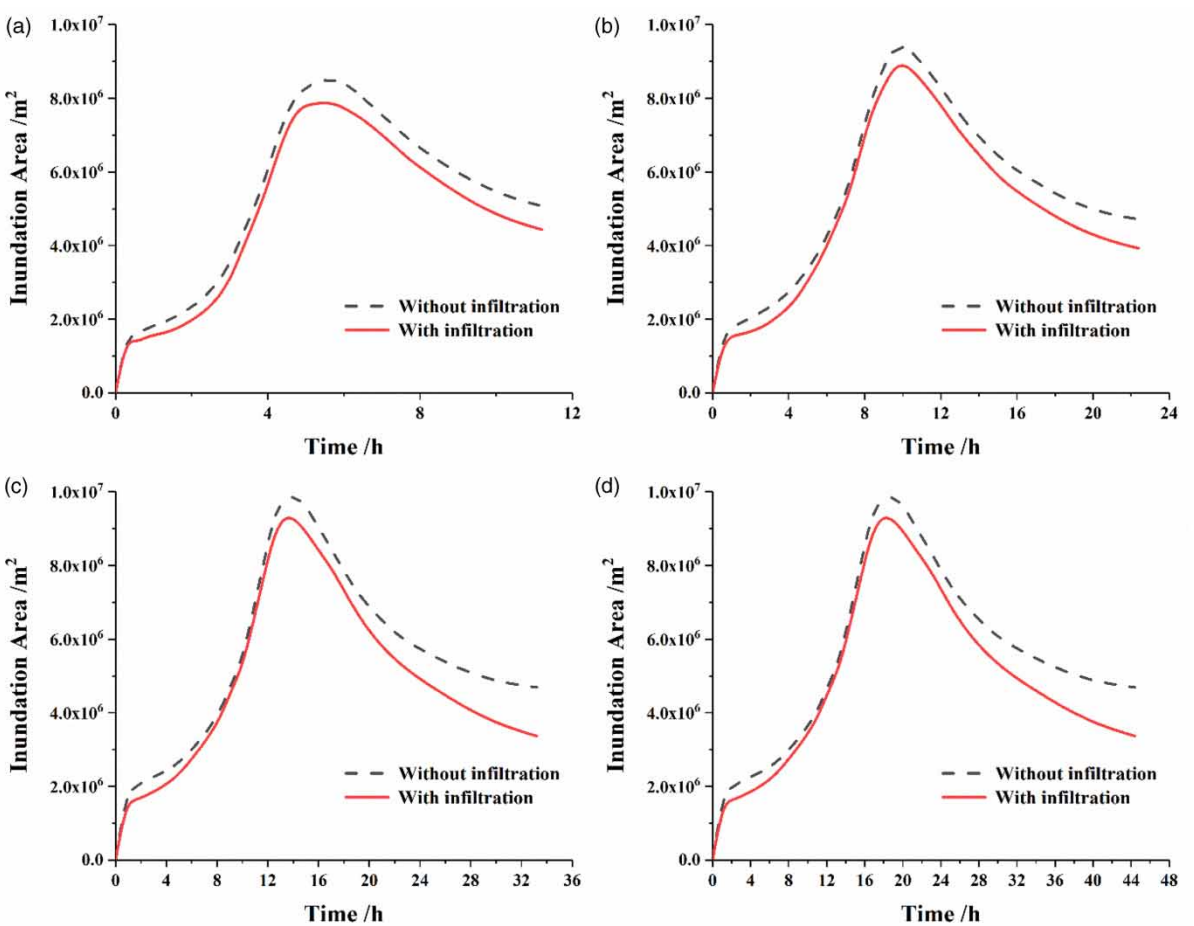

Fig. 9. | Simulated inundation area for different designed hydrographs: (a) $t = 11.1$; (b) $t = 22.2$; (c) $t = 33.3$; and (d) $t = 44.4$ h.

Table 3. | Comparison of the inundation areas computed by the model with/without the infiltration process.

Flood duration (h)	11.1	22.2	33.3	44.4
Relative error (%)	12.54	16.69	22.23	28.20

farmland submerged; when the flood recedes, the flow in the river channel decreases, and the water on the bank gradually returns to the river channel (Pan *et al.*, 2012).

The simulation results in Section 4.1 show that for the fully hydrodynamic model, the flood propagation process is effectively simulated, and the influence of infiltration on the simulation results is related to the peak shape coefficient of the flood. Notably, the peak shape coefficient mainly reflects the flood curve shape before a flood peak. The smaller the peak shape coefficient is (i.e., closer to 0), the faster the flood depth is rising, and the more land that will contribute to infiltration. This is because when the peak shape coefficient is small, the flood will reach the peak discharge in a short time, which makes more land begin the infiltration process in advance, thus increasing the amount of infiltration; however, when the peak shape coefficient increases, the rising speed of a flood slows, and the time of land-based infiltration is delayed. When the flood duration remains constant, the more extensive the process of land infiltration is, the greater the difference in the final inundated area is.

The simulated results in Section 4.2 show that the flood duration has some effect on the inundation area of the flood. Because the infiltration is a hydrological process, when infiltration occurs in a certain area, the amount of infiltration increases with time when the soil is unsaturated. Therefore, when the peak shape coefficient remains unchanged and the flood duration increases, that is, the infiltration time is prolonged, which means that more water is consumed in soil infiltration, and the difference of inundation area is larger (Xie & Fan, 2004).

However, in Sections 4.1 and 4.2, the main reason for the difference in the final inundation area may be that after the completion of the flood recession, there is some water trapped in the depressions and puddles at the flooded area. If the infiltration is not considered, such water will be counted as the submerged area, while under the condition of infiltration, such water will disappear with the infiltration, resulting in the difference of inundation area.

When using a model to create flood risk maps or forecast flood routing, the calculation efficiency is a very important standard. When the accuracy allows or only the maximum inundation area must be calculated, to improve the model calculation speed and efficiency, infiltration can be neglected. For example, in the calculation of the 'thin and sharp type' flood, the infiltration term can be ignored, which improves the efficiency of the simulation. If a flood disaster suddenly occurs and the incidence of a flood must be quickly simulated for post-disaster rescue efforts, the infiltration term can be ignored according to the inundation standard, and a rescue plan can be quickly obtained. However, to improve the accuracy of the calculation results, the influence of infiltration should be considered in simulations, and we can perform simulation assessments or scientific evaluations of the loss caused by floods.

In this study, the hydrodynamic model coupled with the hydrological process was used for research. Because the GPU acceleration technology was used in the simulated calculation, the operation time of the model can be greatly shortened. Therefore, the research efficiency can be improved, and the research expenditure can be reduced. Besides, the influence of peak shape coefficient and flood duration on infiltration was studied, and some conclusions were drawn, but the influence factors which we consider are still not enough. In the future, more influencing factors will be considered and combined with the physical experiment to study the flood routing.

6. CONCLUSIONS

To study the effectiveness of flood propagation simulations with infiltration, this work uses a fully hydrodynamic model to predict the flood propagation process, and the G-A model is applied to calculate infiltration loss. As a criterion related to the flood impact, the peak shape coefficient and flood duration are used as simulation variables in this paper. The main conclusions are as follows:

- The influence of infiltration on the inundation area is not significant in the rising stage of a flood. For the terrain and input conditions in this paper, the largest gap between the two cases is only approximately 5%.
- In the recession stage, the effect of infiltration appears, and in the falling stage, the influence of infiltration gradually increases. In all the examples of this paper, the biggest difference is 28.2%.
- For the different peak-type coefficients, the influence of infiltration on the inundation area varies. The closer the peak-type coefficient is to 1 h, the smaller the influence of infiltration on the inundation area.
- For inflows with different flood durations, specifically, if other issues are unchanged, the influence of infiltration on the inundated area will change much if the duration of the flood is simply prolonged.

In addition, the study area selected in this paper has a large infiltration coefficient. To ensure the calculation efficiency, if a long-duration flood occurs in an area with a low infiltration rate or the flood time is short, the infiltration term can be ignored in the simulation. The research results provide a reference for flood control and post-disaster rescue. When the decision-maker wants to know immediately the post-disaster rescue plan or the flood risk map, which only needs the simulated result of the maximum inundation area, the influence of infiltration should be ignored to pursue the calculation speed of the flood model. However, the influence of infiltration should be considered when it is necessary to evaluate the loss of flood disaster or study the process of flood recession. In addition, the infiltration effect on the flood simulation may be related to the local topography, underlying surface conditions and Manning coefficient. These need to be studied further in the future.

ACKNOWLEDGMENTS

This work is partly supported by the National Natural Science Foundation of China (No. 51609199), the Shaanxi International Science, Technology Foundation of China (Grant No. 2017KW-014), the National Key Research and Development Program of China (No. 2016YFC0402704) and Key Technologies of Guyuan Sponge City Construction and Operation Program (No. SCHM-2018-0104).

DATA AVAILABILITY STATEMENT

Data cannot be made publicly available; readers should contact the corresponding author for details.

REFERENCES

Ata, R., Pavan, S., Khelladi, S. & Toro, E. F. (2013). A weighted average flux (WAF) scheme applied to shallow water equations for real-life applications. *Advances in Water Resources 62*, 155–172. doi:10.1016/j.advwatres.2013.09.019.

Bazilevs, Y., Hsu, M., Kiendl, J., Wüchner, R. & Bletzinger, K. (2011). 3D simulation of wind turbine rotors at full scale. Part II: fluid – structure interaction modeling with composite blades. *International Journal for Numerical Methods in Fluids 65*, 236–253. doi:10.1002/fld.

Chu, S. T. (1978). Infiltration during an unsteady rain. *Water Resources Research 14*(3), 461–466. doi:10.1029/WR014i003p00461.

Climate Change 2001: Mitigation (2002). Choice Reviews Online 39(08), 39-4638. doi:10.5860/choice.39-4638.

Dutta, D., Herath, S. & Musiake, K. (2006). An application of a flood risk analysis system for impact analysis of a flood control plan in a river basin. *Hydrological Processes 20*(6), 1365–1384. doi:10.1002/hyp.6092.

Engman, B. E. T. & Asce, M. (1986). Roughness coefficients for routing surface runoff.Journal of Irrigation and Drainage Engineering *112*(1), 39–53.

Esteves, M., Faucher, X., Galle, S. & Vauclin, M. (2000). Overland flow and infiltration modelling for small plots during unsteady rain: numerical results versus observed values. *Journal of Hydrology 228*(3–4), 265–282. doi:10.1016/S0022-1694(00)00155-4.

Fernández-Pato, J., Caviedes-Voullième, D. & García-Navarro, P. (2016). Rainfall/runoff simulation with 2D full shallow water equations: sensitivity analysis and calibration of infiltration parameters. *Journal of Hydrology 536*, 496–513. doi:10.1016/j.jhydrol.2016.03.021.

Guan, M., Wright, N. G. & Sleigh, P. A. (2014). This is a repository copy of a 2D process-based morphodynamic model for flooding by White Rose Research Online URL for this paper: Version: Accepted Version Article: Guan, M, Wright, NG and Sleigh, PA (2014) A 2D process-based morphodynamic model. *Journal of Hydraulic Engineering 140*(7), 04014022.

Hou, J., Liang, Q., Simons, F. & Hinkelmann, R. (2013a). A 2D well-balanced shallow flow model for unstructured grids with novel slope source term treatment. *Advances in Water Resources 52*, 107–131. doi:10.1016/j.advwatres.2012.08.003.

Hou, J., Simons, F., Mahgoub, M. & Hinkelmann, R. (2013b). A robust well-balanced model on unstructured grids for shallow water flows with wetting and drying over complex topography. *Computer Methods in Applied Mechanics and Engineering 257*, 126–149. doi:10.1016/j.cma.2013.01.015.

Hou, J., Guo, K., Liu, F., Han, H., Liang, Q., Tong, Y. & Li, P. (2018). Assessing slope forest effect on flood process caused by a short-duration storm in a small catchment. *Water 10*(9). doi:10.3390/W10091256.

Hou, J., Han, H., Qi, W., Guo, K., Li, Z. & Hinkelmann, R. (2019). Experimental investigation for impacts of rain storms and terrain slopes on low impact development effect in an idealized urban catchment. *Journal of Hydrology 579*, 124176. doi:10.1016/j.jhydrol.2019.124176.

Hou, J., Kang, Y., Hu, C., Tong, Y., Pan, B. & Xia, J. (2020a). A GPU-based numerical model coupling hydrodynamical and morphological processes. *International Journal of Sediment Research 35*(4), 386–394. doi:10.1016/j.ijsrc.2020.02.005.

Hou, J., Li, B., Tong, Y., Ma, L., Ball, J., Luo, H., Liang, Q. & Xia, J. (2020b). Cause analysis for a new type of devastating flash flood. *Hydrology Research 51*(1), 1–16. doi:10.2166/nh.2019.091.

Hou, J., Wang, N., Guo, K., Li, D., Jing, H., Wang, T. & Hinkelmann, R. (2020c). Effects of the temporal resolution of storm data on numerical simulations of urban flood inundation. *Journal of Hydrology* 125100. doi:10.1016/j.jhydrol.2020.125100.

Hsu, S.-Y. & Hilpert, M. (2011). Incorporation of dynamic capillary pressure into the Green-Ampt model for infiltration. *Vadose Zone Journal 10*(2), 642–653. doi:10.2136/vzj2010.0069.

Jeong, W., Yoon, J. S. & Cho, Y. S. (2012). Numerical study on effects of building groups on dam-break flow in urban areas. *Journal of Hydro-Environment Research 6*(2), 91–99. doi:10.1016/j.jher.2012.01.001.

Lamb, R., Crossley, M. & Waller, S. (2009). A fast two-dimensional floodplain inundation model. *Proceedings of the Institution of Civil Engineers: Water Management 162*(6), 363–370. doi:10.1680/wama.2009.162.6.363.

Li, F. & Zheng, F. (2008). Study on ecological environment influence of different age of hippophae in hilly and gully region on the loess plateau. *Agricultural Research in the Arid Areas 26*, 118–123.

Liang, Q. (2010). Flood simulation using a well-balanced shallow flow model. *Journal of Hydraulic Engineering 136*(9), 669–675. doi:10.1061/(ASCE)HY.1943-7900.0000219.

Marchi, L., Borga, M., Preciso, E. & Gaume, E. (2010). Characterisation of selected extreme flash floods in Europe and implications for flood risk management. *Journal of Hydrology 394*(1–2), 118–133. doi:10.1016/j.jhydrol.2010.07.017.

Meng, S. & Yang, Y. (2019). Infiltration simulation with improved Green-Ampt model coupled with the wet zone partition function. *Journal of Hydrologic Engineering 24*(5), 1–13. doi:10.1061/(ASCE)HE.1943-5584.0001782.

Pan, F. F. & Nichols, J. (2012). Remote sensing of river stage using the cross-sectional inundation area-river stage relationship (IARSR) constructed from digital elevation model data. *Hydrological Processes 27*(25), 3596–3606. doi:10.1002/hyp.9469.

Rawls, W. J., Brakensiek, C. L. & Saxton, K. E. (1982). Estimation of soil water properties. *Transactions – American Society of Agricultural Engineers 25*(5). doi:10.13031/2013.33720.

Simons, F., Busse, T., Hou, J., Özgen, I. & Hinkelmann, R. (2014). A model for overland flow and associated processes within the hydroinformatics modelling system. *Journal of Hydroinformatics 16*(2), 375–391. doi:10.2166/hydro.2013.173.

Valipour, M., Bateni, S. M., Gholami Sefidkouhi, M. A., Raeini-Sarjaz, M. & Singh, V. P. (2020). Complexity of forces driving trend of reference evapotranspiration and signals of climate change. *Atmosphere 11*, 1081.

Westra, S., Fowler, H. J., Evans, J. P., Alexander, L. V., Berg, P., Johnson, F., Kendon, E. J., Lenderink, G. & Roberts, N. M. (2014). Future changes to the intensity and frequency of short-duration extreme rainfall. *Reviews of Geophysics 52*(3), 522–555. doi:10.1002/2014RG000464.Received.

Wu, H., Adler, R. F., Tian, Y., Huffman, G. J., Li, H. & Wang, J. (2014). Real-time global flood estimation using satellite-based precipitation and a coupled land surface and routing model. *Water Resources Research 50*(3). doi:10.1111/j.1752-1688.1969.tb04897.x.

Xie, W. Y. & Fan, G. S. (2004). Influence of soil structure on infiltration characteristics of soil. *Journal of Taiyuan University of Technology* doi:10079432(2004)35:4<381:TRJGDT>2.0.TX;2-C.

Yanwei, F., Wenju, Z. & Yu, W. (2015). Improvement and verification of the Green-Ampt model for sand-layered soil. *Transactions of the Chinese Society of Agricultural Engineering 31*(05), 93–99.

Zhang, H. (2014). *Urban Flood Simulation by Coupling a Hydrodynamic Model with a Hydrological Model.*

First received 10 September 2020; accepted in revised form 4 June 2021. Available online 30 June 2021